



# Conceptual design and FEM structural response of a suspended glass sphere made of reinforced curved polygonal panels

Maurizio Froli · Francesco Laccone

Received: 27 April 2020 / Accepted: 5 August 2020  
© Springer Nature Switzerland AG 2020

**Abstract** The paper introduces a novel concept for structural glass shells that is based on the mechanical coupling of double curved heat-bent glass panels and a wire frame mesh, which constitutes a grid of unbonded edge-reinforcement. Additionally, this grid has the purpose of providing redundancy. The panels have load-bearing function, they are clamped at the vertices and dry-assembled. The main novelty lies in the use of polygonal curved panels with a nodal force transfer mechanism. This concept has been validated on an illustrative design case of a 6 m-diameter suspended glass sphere, in which regular pentagonal and hexagonal spherical panels are employed. The good strength and stiffness achieved for this structure is demonstrated by means of local and global FE models. Another fundamental feature of the concept is that the reinforcement grid provides residual strength in the extreme scenarios in which all panels are completely failed. A quantitative measure of redundancy is obtained by comparing this scenario with the ULS.

**Keywords** Glass shell · Structural glass · Curved glass · Heat bent · Steel reinforcement · Truncated icosahedron · Finite element analysis

## 1 Introduction

Glass is an ideal material for building skins since it provides for transparency, for resistance to weather phenomena or building separation, and also for load-bearing capacity (Haldimann et al. 2008; Feldmann et al. 2014; Belis et al. 2019). All these capabilities can be simultaneously exploited in building elements such as shear walls and roofs as well as in modern building envelopes where wall and roof elements blend in a single piece. Hence, to maximize the transparency, glass panels are exploited to carry additional loading and not only to support their own weight.

A large topological variety and several structural concepts may be found in building envelopes that behave as a single-layer shells. As almost all the materials used in architecture, glass is produced in flat panels of limited sizes and shapes. These flat panels need to be processed in order to tessellate the ideal shell surface, which is segmented in triangle, quad, diamond or polygonal shapes. The selected discretization strategy has direct implications on the geometry and mechanics of the shell. Thus, the actual structure will result in a faceted surface or possibly the panels can be curved to better approximate the target surface.

---

F. Laccone (✉)  
Institute of Information Science and Technologies  
“Alessandro Faedo” (ISTI), Italian National Research  
Council (CNR), Via G. Moruzzi 1, 56124 Pisa, Italy  
e-mail: francesco.laccone@isti.cnr.it;  
francesco.laccone@destec.unipi.it

M. Froli · F. Laccone  
Department of Energy, Systems, Territory and Construction  
Engineering, University of Pisa, Largo Lucio Lazzarino 1,  
56122 Pisa, Italy  
e-mail: m.froli@ing.unipi.it

48 However, few glass-covered shells use glass as a  
 49 structural material, conversely the majority of them are  
 50 grid shells, in which the metal or timber grid serves  
 51 as only load-bearing material (Schlaich and Schober  
 52 1996; Adriaenssens et al. 2012; Feng and Ge 2013;  
 53 Bruno et al. 2016; Wang et al. 2016; Mesnil et al. 2017).  
 54 All these factors make the conceptual design of discrete  
 55 shells a complex problem.

## 56 1.1 Structural glass shells

57 Similarly to other spatial structures (Romme et al.  
 58 2013), structural glass shells can be classified on the  
 59 basis of their structural behavior. In turn, this latter is  
 60 affected by the adopted discretization strategy and the  
 61 joints design.

62 A first group includes structures based on strut-and-  
 63 tie or tensegrity behavior. These systems usually adopt  
 64 triangular or quad panels. Quads are commonly braced  
 65 by cables to increase the cell stiffness. The panels are  
 66 point-fixed at their corners, i.e. with clamping. Hence,  
 67 the structural assembly can be reduced as a discrete sys-  
 68 tem made of axial-only stressed components, similarly  
 69 to a truss. This behavior is favored by the node transfer  
 70 mechanism, which causes compression in glass area  
 71 close to the panels edges that behave as struts, and ten-  
 72 sion on steel components—if present—that perform as  
 73 ties. Exemplars of this structures are the post-tensioned  
 74 dome at Weltbild Verlag building in Augsburg (Wurm  
 75 2007) and the Maximilianmuseum roof (Ludwig and  
 76 Weiler 2000), whose conceptual design has been man-  
 77 aged with a reduced truss model. Recently, the work  
 78 (Laccone et al. 2020) demonstrates how a truss reduced  
 79 model can be employed to derive the automatic design  
 80 of strut-and-tie post-tensioned glass shells.

81 A second group of structural glass shells is based  
 82 on the shell behavior. These systems manifest surface  
 83 resistance and rely on continuous smooth load transfer.  
 84 In fact, the linear joints that are usually adopted to pro-  
 85 vide for an interrupted force transfer between the panels  
 86 edges. While for strut-and-tie shells the nodes are vul-  
 87 nerable zones due to high stress, in the shell category  
 88 stress concentrations are reduced. Again, while for the  
 89 previous category a mesh with high connectivity (tri-  
 90 angle or braced quad) supplies for redundancy; in the  
 91 shell category, faces with high number of edges have  
 92 major redundancy. Typically polygonal panels (quads  
 93 or hexagons) are adopted for the group based of shell

94 behavior. Exemplars of these structures are the Delft  
 95 dome (Veer et al. 2003), the Blandini's dome (2005;  
 96 2008) and the Plate shell structures (Bagger 2010).  
 97 Recent work demonstrates that a post-tensioned spher-  
 98 ical glass shell can span up to 26 m (Hayek et al. 2018).

## 99 1.2 Heat-bent curved glass

100 While flat glass is employed in a significant amount  
 101 of building applications, bent glass has become more  
 102 appealing in architectural contexts in which curved  
 103 forms and continuous reflectivity must be ensured  
 104 (Neugebauer 2014). Glass can be bent following two  
 105 main approaches: cold bending, based on forcing and  
 106 restraining flat panels in situ or during lamination; and  
 107 heat bending, based on forming new shapes of panels  
 108 through heating panes up to about 600 °C (Timm and  
 109 Chase 2014).

110 The gravity bending or slumping is the traditional  
 111 and commonly used process for thermally bent glass.  
 112 It is based on heating a pre-cut flat panel that is laid  
 113 over a bespoke mould. The high temperature soften the  
 114 glass while it sinks into the mould due to its own weight.  
 115 The panels show good optical quality and absence of  
 116 anisotropies. All shapes from single to double curved  
 117 are feasible. On the other hand, tempering or heat  
 118 strengthening process are problematic since they would  
 119 alter the original forming. So, chemical strengthening  
 120 and lamination after the bending process are recom-  
 121 mended to provide a fail-safe behaviour.

122 A money-saving process is the online bending,  
 123 which consists in providing one-axis curvature through  
 124 a robotic press while the pane is heated in a furnace  
 125 and pass through it. Apart for time-efficiency, another  
 126 advantage is that the online bent glass becomes either  
 127 fully tempered or heat strengthened during the bending  
 128 process itself.

129 Thus, while the online bending is used for mass pro-  
 130 duction, the gravity bending ensure the best surface  
 131 condition and aesthetic quality (Fildhuth et al. 2018).  
 132 The façade of La Maison des Fondateurs represent an  
 133 example of using gravity bent glass panels (Villiger  
 134 et al. 2019). These panels perform as separation walls  
 135 and as load-bearing elements for both vertical and hor-  
 136 izontal forces. In fact, because of the shape stiffness, a  
 137 curved glass is particularly suitable for application in  
 138 shell structures.

### 139 1.3 Objectives of the present work

140 Strut-and-tie structures have been already built in large  
 141 scale exemplars and appear reliable enough since they  
 142 are tested also in extreme failure scenarios, such as the  
 143 complete collapse of some panels. On the other hand,  
 144 the opportunity offered by the shell structure to use  
 145 polygonal panels is more appealing from an architec-  
 146 tural viewpoint because of the reduction of the opaque  
 147 parts (such as panels edges, seals, reinforcement and  
 148 nodes) that brings to an increased transparency.

149 The present work introduces a novel structural con-  
 150 cept for glass shells made of polygonal panels that are  
 151 supported at the vertices and reinforced at the edges by  
 152 means of unbonded steel rods, combining the features  
 153 of both categories of structural glass shells. The con-  
 154 cept derives from Froli and Laccone (2018), but, apart  
 155 from the use of curved polygonal panels, it differs from  
 156 this latter because no post-tensioning is provided as it  
 157 would lead to a premature buckling failure of curved  
 158 glass panels.

159 Reinforcing a tensioned glass panel edge is a  
 160 commonly-adopted strategy to mitigate the conse-  
 161 quences of brittle failures. This steel component is  
 162 usually bonded or embedded to adhere to glass and  
 163 to achieve a safer post-cracking phase (Martens et al.  
 164 2015a; Louter et al. 2012; Martens et al. 2016; Cupac  
 165 et al. 2017); the unbonded configuration is more com-  
 166 mon in post-tensioned glass structures (Froli and Lani  
 167 2010; Martens et al. 2015b; Bedon and Louter 2016;  
 168 Engelmann and Weller 2016). In the present case, deal-  
 169 ing with a shell structure, the reinforcement has also a  
 170 purpose of adding redundancy and avoid global col-  
 171 lapse. So, it has to be stiff enough in both tension and  
 172 compression, and consider the complete failure of pan-  
 173 els.

174 The present concept has been tested on an illustra-  
 175 tive case study of a Suspended Glass Sphere (SGS).  
 176 The structure has been conceived by the author Froli  
 177 for outdoor use with the aim of hosting a particular  
 178 art installation in the inside (Fig. 1). It pursues the  
 179 necessity of guaranteeing an all-round vision of the art  
 180 object through the transparent and floating envelope,  
 181 while preserving its functional requirements, such as  
 182 protection from weather phenomena and accessibility  
 183 for maintenance.

184 Although the surface is geometrically defined, its  
 185 structural behavior is not trivial and presents several  
 186 complexities given by the positioning of the panels and



**Fig. 1** 1:10 Scale model demonstrator of the SGS (model by the author Froli)

the response of the whole structure with respect to the suspension system.

To state the feasibility of the structure and to validate the structural concept local and global analyses are performed. In the preliminary design phase a reduced model of the glass panels is adopted. Then, detailed local analyses have been performed.

## 2 Conceptual design and structural system

### 2.1 Structural concept

The static concept is founded on the collaboration of a wire frame steel structure with spherical bent laminated glass panels (Fig. 2). The steel grid is made of rods that merge in three-way nodes by means of a concentric bolt. Additionally, these nodes are shaped to clamp the vertices of glass panels.

Given these boundary conditions, a nodal load-transfer is expected. Therefore, on a global-level the main loading path is aligned with the edge of the starting mesh and consequently the rods can be either tensioned or compressed. Since the panel corner is not glued but it is simply supported in a dry clamped node, no tension can be transferred to glass. If the ideal edge stretches, tension flows on the rod only; if it shrinks, the rods and the adjacent glass panels work in parallel (Fig. 3).

Apart from aesthetic reasons, the panel double curvature is a local-level strategy to stiffen the glass. Indeed, as long as the nodes are kept in a fixed posi-

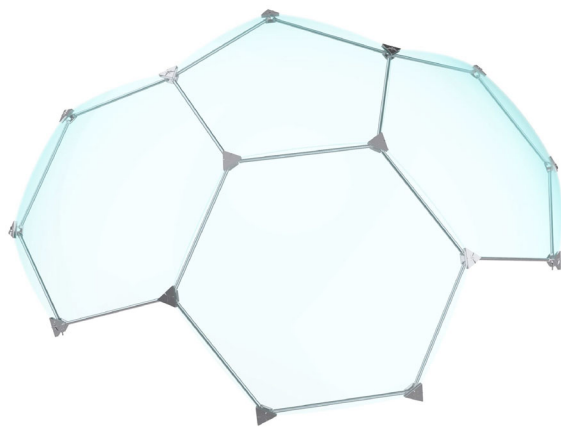
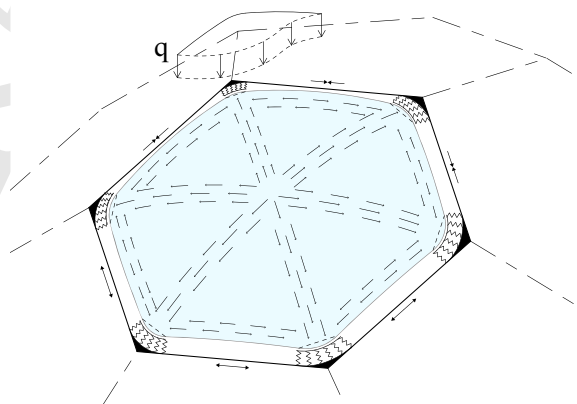


**Fig. 2** Concept of structural system: bent panels and wire frame steel mesh are connected at the nodes; the panels' edges are then sealed for waterproofing

215 tion by a polygon of steel rods, the curved glass panel  
 216 is well supported and can act as a load-bearing shell  
 217 element. The obtained advantage is to have a stiffer  
 218 element compared to what it would be in the case of flat  
 219 panels. Moreover, the panels are considered as lami-  
 220 nated for a safe fail.

221 The panels vertices are rounded to avoid peak stress  
 222 concentration and to allow small and reversible dis-  
 223 placements under dynamic loads to dissipate energy  
 224 as performed by Travi Vitree Tensegrity (TVT) proto-  
 225 types during the experimental tests (Froli and Mamone  
 226 2014). Even though the dynamic aspect is not specifi-  
 227 cally addressed in this work, it is important to see  
 228 it as part of the conceptual design. The dynamics of  
 229 glass structures and its interaction with other structural  
 230 components are becoming an important research topic

**Fig. 3** Free body diagram for the static behavior of reinforced curved polygonal panels



(Bedon et al. 2018; Bedon and Amadio 2018; Santar-  
 siero et al. 2019; Casagrande et al. 2019).

## 2.2 Redundancy concept

Redundancy is a fundamental requirement in glass  
 shells (Engelmann et al. 2017) and should consider sce-  
 narios in which glass is cracked.

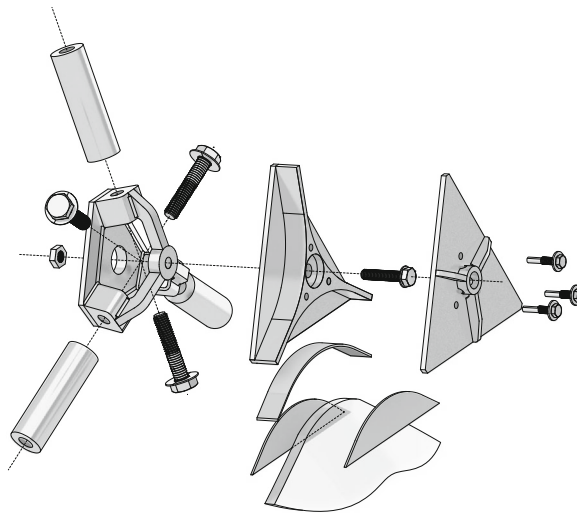
Regarding the geometry, using a polygonal tessella-  
 tion of the ideal glass surface offers in general a redun-  
 dant design solution. In fact, in case of glass cracking,  
 having five or six panels in adjacency, alternative load  
 paths may develop. However, a discontinuity on a single  
 node has the effect of weakening the shell behavior.  
 This is the reason why the grid of reinforcement is  
 paramount to avoid these local failures to propagate in  
 global collapses. The grid provides a lower-bound or  
 residual stiffness level.

Evaluating the redundancy from considerations at  
 local level may be very difficult. On the other hand,  
 a more straightforward approach can be adopted con-  
 sidering an extreme failure scenario ('worst case sce-  
 nario') in which all panels are supposed collapsed (Froli  
 and Laccone 2018). Therefore, collapsed panels are not  
 able to carry shell forces but only to transfer loads to  
 the vertices. This behavior is mechanically akin to a  
 grid shell and can be easily simulated.

## 2.3 Joint design

The node is the fundamental component of the sys-  
 tem since it does accomplish several requirements. The

**Fig. 4** Conceptual design of the node for the SGS



node is inspired by the TVT nodes (Froli and Mamone 2014), which have been designed for post-tensioned glass beams. A conceptual view of the node designed for the SGS is in Fig. 4. This node is built on two levels: the lower one to connect the rods; the upper one to connect the vertices of panels. The two groups of structural elements can be slightly spaced without inducing any geometrical distortion on the node, and with the advantage of presenting only the glass surface on the outside of the shell to benefit from a continuous reflectivity and water-tightness.

The valence 3 node has fostered a compact and aesthetically pleasant design in spite of the demand of stiffness, strength, dry-assembly moving spaces that on the other hand are more easy to accomplish with an oversized component.

Like TVT nodes, the glass to steel contact is avoided by the interposition of softer material such as aluminium type EN AW-6060 T5 and polyethylene. Moreover, these spacers have to consider the tolerances of panels and to guarantee the contact of steel and glass at the assembly phase. The tolerance of glass panels is the weakest point in the system and is related with the outline precision and in turn with the accuracy of bending and lamination. This tolerance should be within the limit of  $\pm 3$  mm (Bundesverband Flachglas 2011), but also higher values of  $\pm 5$  mm have been experimentally found (Bukieda et al. 2018). The control of bending geometry constitutes the major issue. It is recommended to realize prototypes to be surveyed and tested with real load scenarios. If larger tolerances are

found on the prototypes, then the node design has to be updated in order to include additional adjustment capability, to embed thicker spacer material or to increase the clamping area. These scenarios affect the structural behavior of the connection, which is to be tested and better characterized in order to update the FE model.

The current node has been verified for robustness, namely to be over resistant with respect to the forces transferred from the incident elements. Moreover, the feasibility of all the assembly movement have been checked since one of the strengths of this system is the dry assembly, which favors an easy construction and replacement of damaged components.

### 3 Case study description, analysis method and materials

#### 3.1 Geometry of the SGS

In terms of geometry, the present case study is obtained from a sphere with 6 m-diameter. This surface is segmented with a regular tessellation producing the truncated icosahedron, which is an Archimedean solid, one of 13 convex isogonal nonprismatic solids whose faces are two or more types of regular polygons. In this case, there are 12 all-equal regular pentagonal faces, 20 all-equal regular hexagonal faces (Pottmann 2007). Regular polygons are equilateral and equiangular.

The geometrical approach to generate the truncated icosahedron is the typical tessellation sequence that starts from the icosahedron solid and cut each vertex by

**Fig. 5** Geometric construction of the truncated icosahedron from the icosahedron

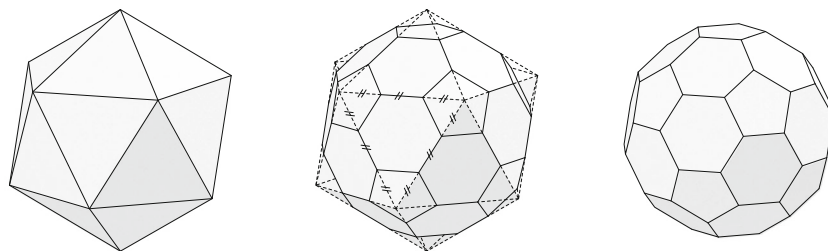


**Table 1** Metrics of the suspended sphere case study

	Unit	Value
Area	m <sup>2</sup>	106.30
Volume	m <sup>3</sup>	97.95
Diameter	mm	6000
Mesh edge length	mm	1210
Num. edges		90
Num. pentagon faces		12
Num. hexagonal faces		20
Num. nodes		60
Node valence		3

Area and Volume are referred to the truncated icosahedron as per Eq. 1

means of a plane, whose normal is equal to the vertex normal (Fig. 5). Two possible solids can be derived: the truncated icosahedron with constant face area and the truncated icosahedron with constant edge length. This latter strategy has been selected and, in particular, the planes divide the original icosahedron edges in three segments. Some of the main quantitative information such as area  $A$  and volume  $V$  can be evaluate analytically from the edge length  $l$  (Eq. 1). The main measures of the case study are included in Table 2.

$$A = \left( 30\sqrt{3} + 3\sqrt{25 + 10\sqrt{5}} \right) l^2 ;$$

$$V = \frac{1}{4} \left( 125 + 43\sqrt{5} \right) l^3 \quad (1)$$

**Table 2** Geometry of the two types of panels

	Area (m <sup>2</sup> )	Circumscribed circle radius (mm)	Rise (mm)	Vertex angle (deg)
Pentagon	2.69	2060	165	108
Hexagon	4.12	2421	255	120

The truncated icosahedron has 60 all-equal vertices of valence 3. After the truncation the nodes valence goes from 6 to 3 with a beneficial effect on the design of connections for low valence nodes (Table 1).

The vertices and the edges of the truncated icosahedron are selected as nodes and as unbonded reinforcement of the structure respectively. The panels of the structure are obtained by projection of the faces on the sphere that pass through the vertices of the solid. Thus, both the reinforcement and the panel vertices merge in the same set of nodes. The faces of the structure are double curved spherical panels of 3 m radius, their main dimensions are included in Table 2 and illustrated in Fig. 6. All panels have rounded vertices of radius 100 mm.

The structure is supported by a suspension system made of 5 masts and a net of cables, which emphasizes the weightless appearance of the sphere, which has a mass  $m = 6600$  kg. The cables are fastened to 10 nodes of the sphere, of which 5 belong to the lower pentagon of the structure. These lower-pentagon nodes are not directly attached to the cables but are sustained by a pentagonal steel ring. From the dynamic point of view, this support system constitutes a decoupling of the sphere motions from the foundation, which could result useful to decrease the demands for earthquake or wind excitation. A rendered view of the SGS is in Fig. 7.

**Fig. 6** Geometry of the regular pentagonal and hexagonal panels used in the SGS

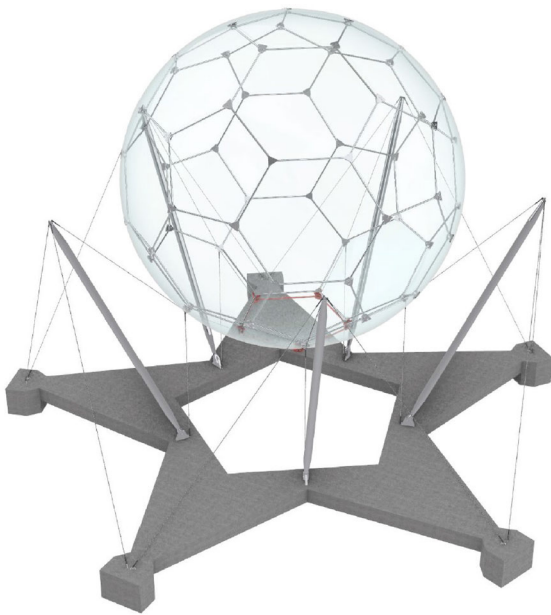
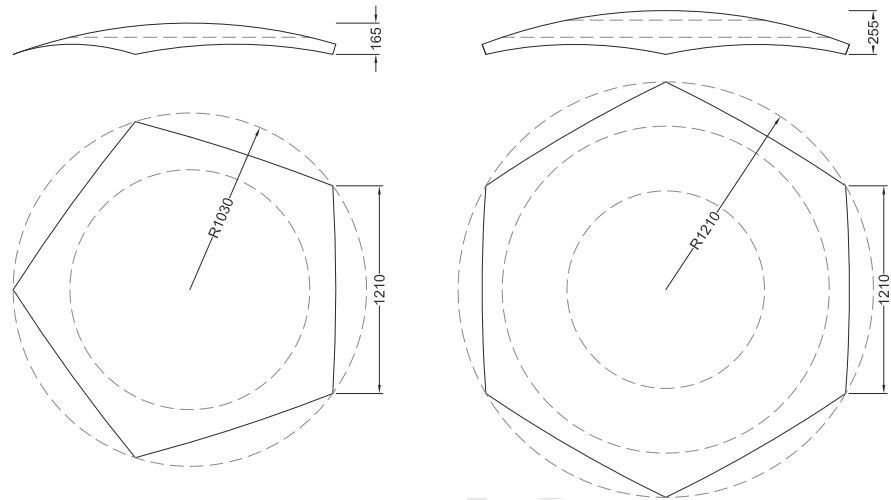


**Fig. 7** Impression of the SGS case study in a urban environment

the robustness evaluation in the ‘worst case scenario’ (WCS). Then, a full detailed model is built and all load combinations are explored.

Depending on the conceptual design and on the employed joints, the panels are expected to perform a rocking dynamic motion within their polygonal frame. This effect is neglected in the present case study as it goes beyond the objectives of the work. However, a dynamic model has been created to study the natural frequencies of the system. In this model, the whole sphere is considered as rigid system.

The following sections are organized to include models and results for each level of investigation. Although they are based on the SGS geometry, local analyses in Sect. 4 and global analyses in Sect. 5 present approaches and results that can be extended to other case studies based on the present concept. Instead, the content of Sect. 6 pertains the suspended systems which are not necessarily related to glass shells.

All FE models are realized by means of a commercial software (G+D Computing 2005, 2010).

### 3.2 Analyses

The validation of the proposed concept is tackled at two levels of investigation: local and global level. The local level analyses regard the structural response of regular pentagonal and hexagonal panels in terms of stress, displacement and buckling. An additional outcome is the calibration of a reduced truss model to be used for design purposes in the global level analyses. This latter regards the static response of the whole structure and

### 3.3 Materials

Glass and common structural steel are the two materials considered in the simulations. The glass panel is made of two plies of 10 mm glass, which are gravity bent, chemically strengthened and laminated with interposed a 1.52 mm PVB layer. Detailed specifications are included in Table 3. All the materials have been defined as isotropic linear elastic.

**Table 3** Components and material adopted for the FE models

Component	Material	Type	Size/cross section	Mech. Parameters
Glass panels	Bent, laminated	CS	10 + 1.52 + 10 mm	$E_g = 70$ GPa; $\nu = 0.23$
Reinforcement rods	Structural steel	S275	$D = 33.7$ mm; $s = 3.2$ mm	
Pentagonal ring	Structural steel	S275	$D = 76.1$ mm; $s = 5.0$ mm	$E_s = 210$ GPa; $\nu = 0.3$
Masts	Structural steel	S275	$D = 168.3$ mm; $s = 10$ mm	
Cables	Steel		$D_{eq} = 18$ mm	$E_c = 200$ GPa; $\nu = 0.3$

CS stands for chemically strengthened

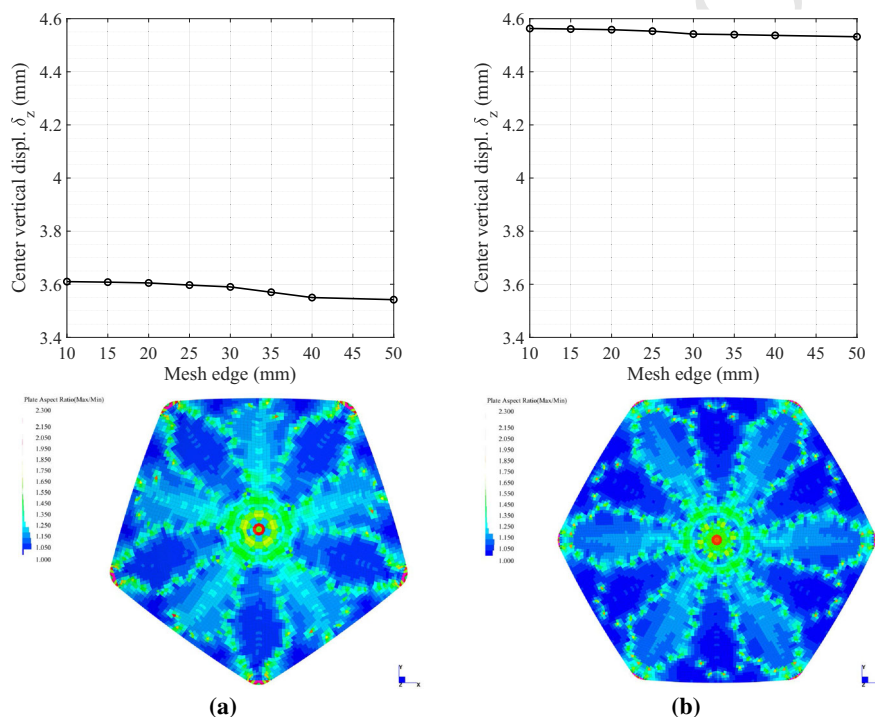


**Fig. 8** Sensitivity analysis of FE plate model of the bent glass panels at the top and aspect ratio contour map of the 20 mm-edge-size mesh: **a** pentagon, **b** hexagon

## 396 4 Structural response of polygonal doubly-curved 397 glass panels and reduced model calibration

### 398 4.1 Model

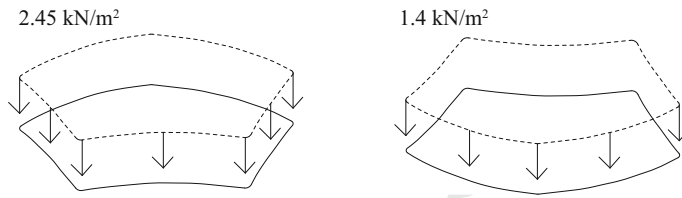
399 The bent glass panel has been modeled as FE plate  
400 shell elements with an edge size dimension of 20 mm  
401 (Fig. 8). For this single-ply model, the equivalent thick-  
402 nesses of glass have been used. The calibration of the  
403 boundary condition is the most demanding part of the  
404 work. In the absence of experimental data, the stiffness  
405 of the compression-only contact elements is deduced

406 as done for the TVT connections on the basis of the  
407 spacer material.

408 Geometrical and contact nonlinearities are consid-  
409 ered in the analysis. The following calculations are pre-  
410 formed in the worst condition for geometry and load  
411 within the SGS. In particular, there are three extreme  
412 representative loading conditions for both panels: (a)  
413 the panel is in a concave position, i.e. at the top of  
414 the structure, with gravitational load and snow; (b)  
415 the panel is in a convex position, i.e. at the bottom of the  
416 structure, with gravitational load; (c) the panel that has  
417 one or more vertices on the supports, in this case an  
418 asymmetrical reaction force is to be summed to face



**Fig. 9** Geometry and loads on panels: **a** convex, **b** concave position



loading. Among the three, the case (a) is the better performing and the case (b) is the worst condition (Fig. 9), therefore case (c) is omitted for sake of brevity.

stress is almost null, in the concave position it reaches the value of  $\sigma_{11} = 29.4$  MPa because the panel behave as a tensile membrane.

#### 4.2 Stress and displacement results

The results of conditions (a) and (b) are shown in Fig. 10, from which it is possible to show how different is the behavior of the panels in both cases due to the shape effect. While in the convex position tensile

For the deformations, the support nonlinearity is decisive. The convex panel is well supported by the compression-only support and then result very stiff. On the other hand, the concave panel suffers from a less stiff clamping reactions. This effect appear even more enhanced considering that the SLS load on the concave panel is about half of that on the convex one. However, even considering the limitation of CNR (2012)

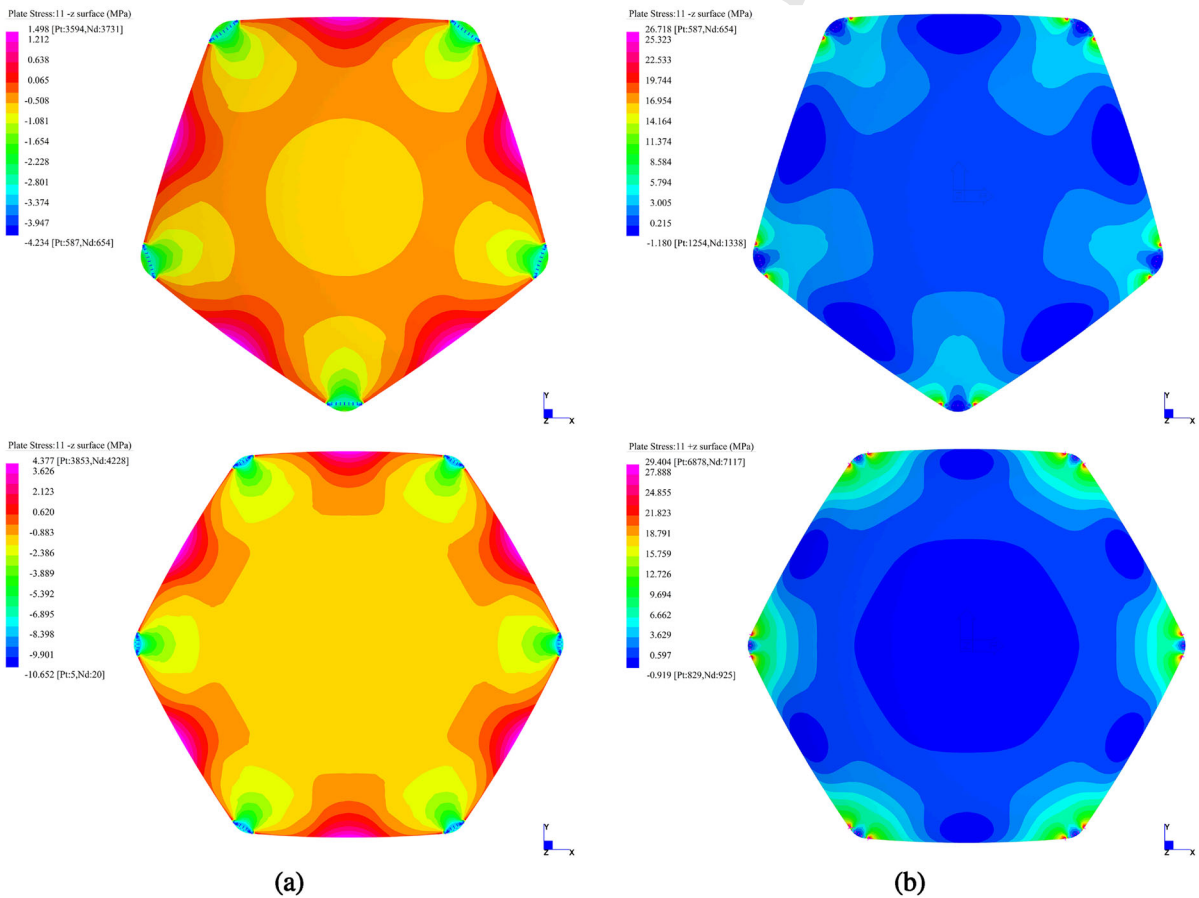


**Fig. 10** Maximum principal stress results for panels in **a** convex, **b** concave position

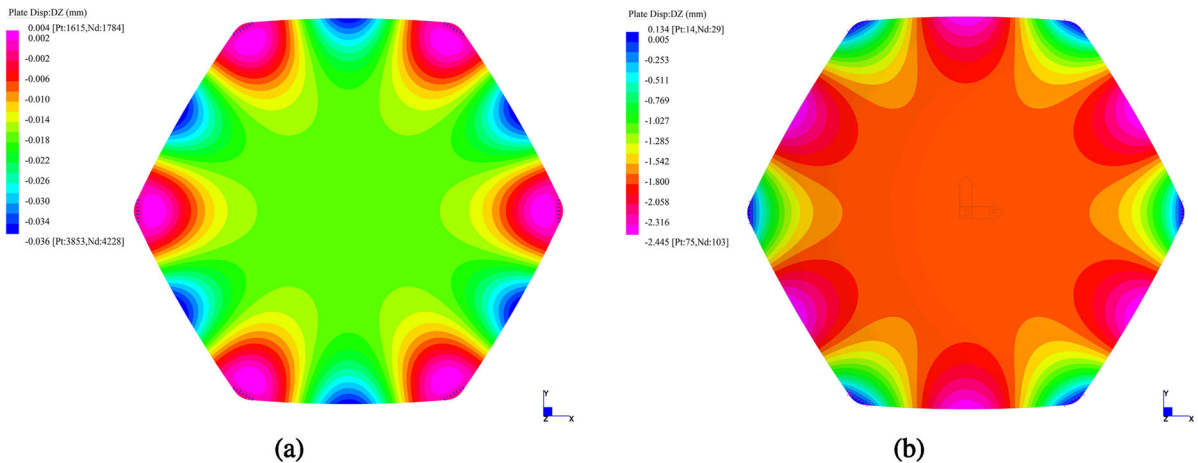


**Fig. 11** Deformation for the hexagonal panels in **a** convex, **b** concave position

438  $i/100 = 12.1$  mm the maximum deflection of the con-  
 439 vex panels results well within this limit.

#### 440 4.3 Buckling

441 For compressed panels, a risk to prevent is to have  
 442 a buckling failure for design loads. Although exten-  
 443 sive literature has been developed on glass buckling  
 444 (Bedon and Amadio 2014; Bedon et al. 2015; López-  
 445 Aenlle et al. 2016; Bedon and Amadio 2016; Luible  
 446 and Schärer 2016; Liu et al. 2017; D'Ambrosio and  
 447 Galuppi 2020) including cold bent glass performances  
 448 (Galuppi et al. 2014), heat curved panels seems to be  
 449 not investigated. Due to the impossibility to rely on  
 450 realistic methods, a first attempt can be to look at ana-  
 451 lytical solutions and make safe assumptions (Fig. 11).

452 To be on the safe side, the buckling analysis could be  
 453 performed at the layered limit, so on a single ply of the  
 454 panel, neglecting the contribution of the interlayer and  
 455 the collaboration with the twin panel. A closed form  
 456 solution of the buckling load (Timoshenko and Gere  
 457 2012) for shallow spherical cap shell with pin supports  
 458 and a uniformly distributed pressure is given in Eq. 2.

$$459 q_{cr} = \frac{2E}{\sqrt{3(1-\nu^2)}} \left(\frac{t}{R}\right)^2 \quad (2)$$

460 The values of  $t = 10$  mm and  $R = 3$  m are adopted.  
 461 However, neither the boundary conditions nor the result  
 462 is satisfying because in the first case, the actual panel  
 463 is point supported, and in the second case, an upper  
 464 bound for the solution was expected but the equation

led to a value of  $q_{cr} = 930$  kN/m<sup>2</sup> that equals to a load  
 multiplier of 379.6, namely number of times the design  
 pressure on the concave panel 2.45 kN/m<sup>2</sup>. This results  
 is too high to be regarded as plausible.

The FEM linear buckling analysis led to a more real-  
 istic yet still very high value of the buckling factor  
 $\lambda = 12.53$ , taking as initial condition the load on the  
 convex hexagonal panel. Realistic boundary conditions  
 are included.

Again, the obtained value is not physically plausible  
 because if the panel is loaded by the critical buckling  
 load using a static solver it can be observed that the  
 maximum principal stress is far beyond the character-  
 istic strength of the material. It means that the panel  
 tensile failure occurs before buckling. From an incre-  
 mental nonlinear analysis of the panel, the character-  
 istic strength is reached for a load multiplier of 3.15. Also  
 in the case of asymmetrical loading conditions, glass  
 tensile failure remains the most likely failure modal-  
 ity; these scenarios need to be checked via incremental  
 nonlinear analysis.

Further investigations are needed to confirm these  
 preliminary results and most importantly to include the  
 panel imperfections that are to date unknown and have  
 been neglected.

#### 4.4 Stiffness-based reduced model calibration

One of the main advantages of using a point-supported  
 panel as single structural unit is that it can be reduced  
 into an assembly trusses, whose elements are incident

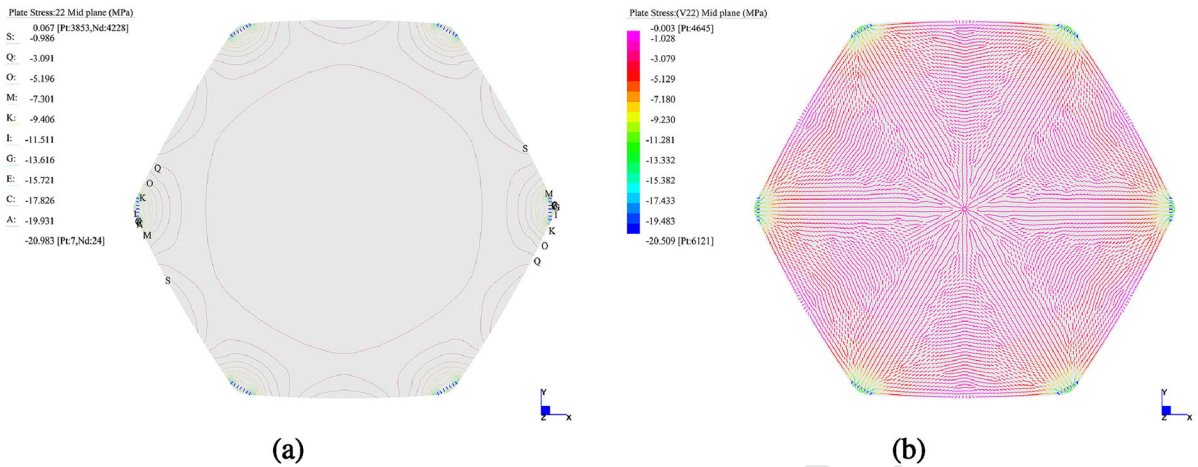


**Fig. 12** Minimum principal stress on the hexagonal panel: **a** isolines; **b** vector field

**Fig. 13** Stiffness-based reduced truss model for **a** the pentagon and **b** the hexagonal panel

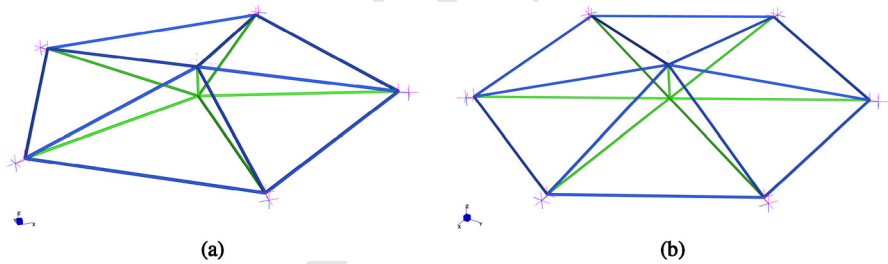


**Table 4** Adopted cross section in the glass panels' reduced model

Component	FE type	Material	Cross section/stiffness	Mech. Parameters
Hexagon blue edges	Truss	Glass	Round $D = 15.3$ mm	$E_g = 70$ GPa; $\nu = 0.23$
Pentagon blue edges	Truss	Glass	Round $D = 15.2$ mm	$E_g = 70$ GPa; $\nu = 0.23$
Green edges	truss	Glass	Round $D = 13.0$ mm	$E_g = 70$ GPa; $\nu = 0.23$
Link to the main node	point contact	–	$k = 560$ kN/m	(Compression only)

Reference to colors of Fig. 13

494 into the support nodes. This is justified by the resulting  
 495 stress paths on the shell element (Fig. 12). In other  
 496 works concerning polygonal tessellations such as Froli  
 497 and Laccone (2017), a fan-shaped truss grid has been  
 498 used to simulate the stiffness contribution of plexiglass  
 499 panels that infill Voronoi meshes.

500 For the present structural concept, a simply fan-  
 501 shaped truss with the central node located on the panel  
 502 center would have been very sensitive to support condi-  
 503 tions and non-membrane loading, and so not represen-  
 504 tative of the actual behavior. Therefore, it is added to a  
 505 second flat layer of truss (i.e. in this case this is equal to

a projection on the flat face) and ring elements. Thus, 506  
 a volumetric tetrahedral structure is formed, and the 507  
 shape stiffness given by double curvature is suitably 508  
 modeled. The model is represented in Fig. 13 while 509  
 the geometric and mechanical properties adopted are 510  
 included in Table 4. 511

A comparison based on the stiffness of the two mod- 512  
 els (the plate and the reduced truss) is used to cali- 513  
 brate the size of the truss elements. A stress criteria 514  
 has indeed no meaning since stress verification can be 515  
 executed on more accurate plate models. The springs 516  
 at the vertices are equivalent to the nonlinear supports 517

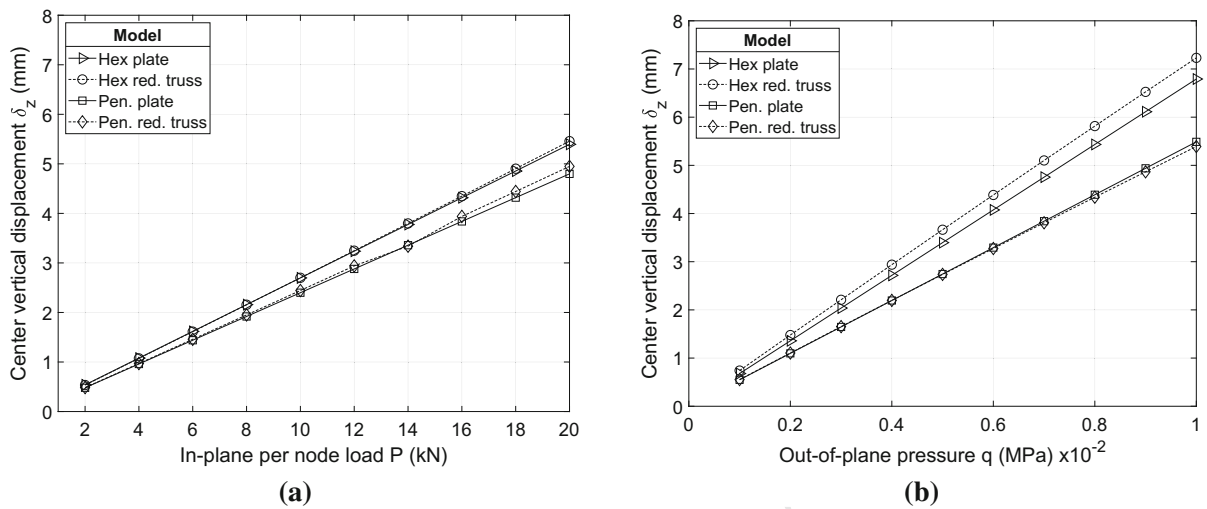
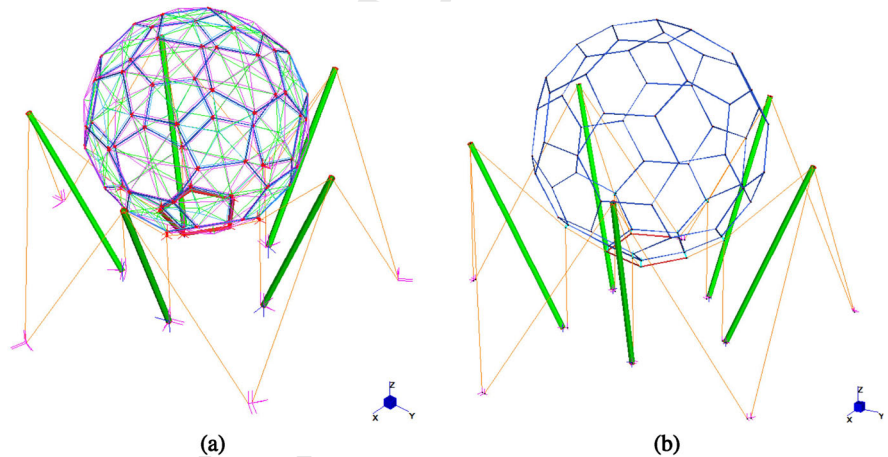


**Fig. 14** Stiffness calibration of the reduced models: **a** in-plane load; **b** out-of-plane load

**Fig. 15** Global models: **a** full model with reduced truss as glass panels; **b** worst-case scenario model



518 of the plate model. The calibration has been executed  
 519 for both in-plane and out-of-plane loading. In the first  
 520 case, the vertices are loaded with forces that are within  
 521 the range of the expected reactions at the supports. In  
 522 the second case, the truss is loaded with vertical load-  
 523 ing equivalent that are equal to the total face pressure  
 524 divided in proportion to the Voronoi area of the mesh  
 525 (Fig. 14).

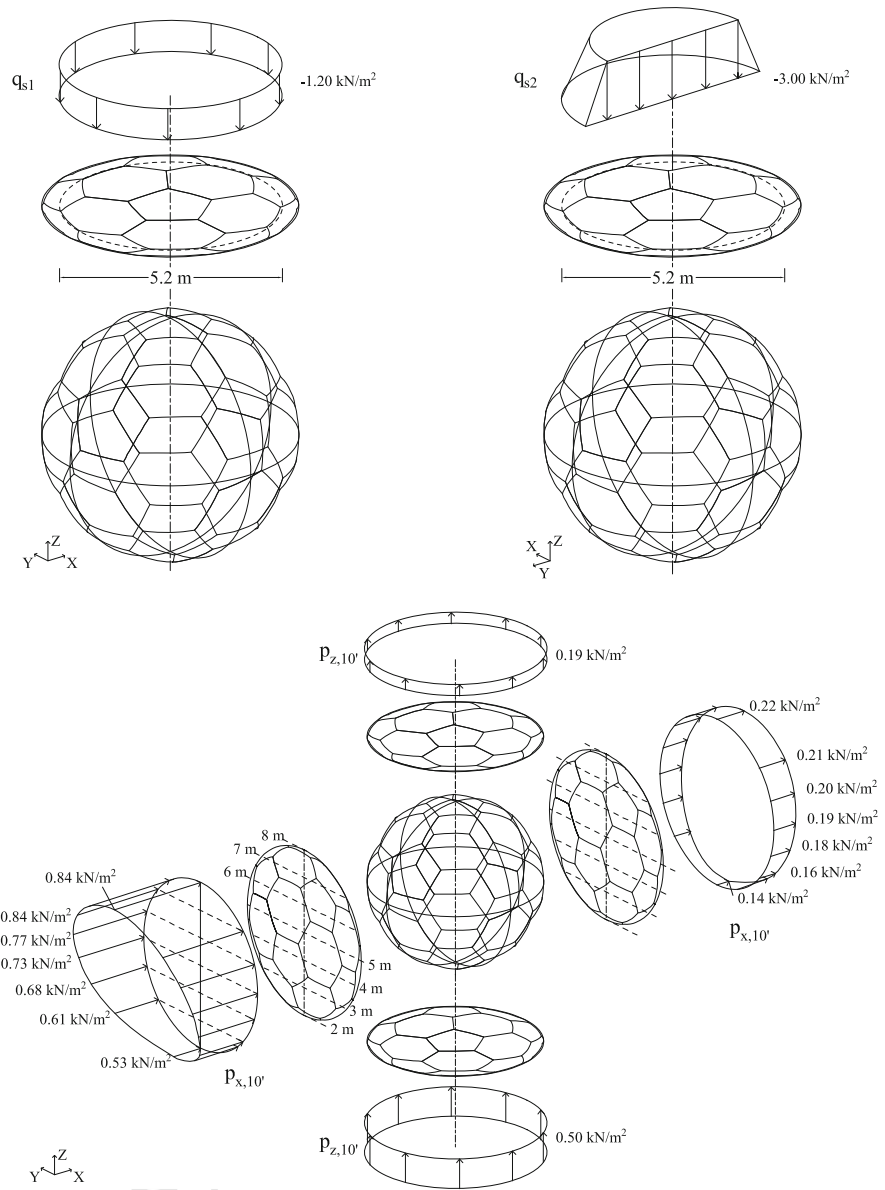
526 The reduced model is employed into the design of  
 527 the truss and the estimation of the WCS performance  
 528 of the structure.

## 5 Global analyses 529

### 5.1 Model 530

531 In a first stage, a global model of the SGS is built  
 532 (Fig. 15) in order to design the steel components. A  
 533 reduced model as per Sect. 4.4 is employed to describe  
 534 the stiffness of bent glass panels. Beam elements are  
 535 used for the rods and for the masts, cut-off bar elements  
 536 are used for the cables. Cross sections and material as  
 537 per Table 3 are used. Nonlinear spring dampers simu-  
 538 lates the connection of the panels vertices with the  
 539 steel nodes.

**Fig. 16** Model and loads on the global model: at the top left, symmetric snow load  $Q_{snow,sym}$ ; at the top right asymmetric snow load  $Q_{snow,asym}$ ; at the bottom  $10'$  wind load  $W_{10'}$



540 The loads are applied on the vertices of the truss that  
 541 represent the panels in proportion to the Voronoi area.  
 542 Geometrical and contact nonlinearities are considered  
 543 in the analysis, while materials are assumed linear. In  
 544 this phase, gravitational and wind loading in X direc-  
 545 tion ( $W_{x,3'}$ ) are used. Their intensity and geometry is  
 546 later specified (Figs. 16, 17).

547 In order to make comparisons with the ULS, another  
 548 model named WCS has been realized to simulate the  
 549 ‘worst case scenario’. In this model, the panels are sup-  
 550 posed to be cracked and unable to play any structural

551 role, except to transfer loads on the steel nodes. There-  
 552 fore, they are removed and their load is directly posi-  
 553 tioned on the nodes.

554 With the aim of testing the response of the structure  
 555 with respect of all kind of loads, a full detailed model is  
 556 developed. This model includes the panels as FE plate  
 557 elements with equivalent thickness. The applied loads  
 558 are schematically represented in Figs. 16, 17 and are  
 559 combined according to the scheme of Table 5. Since  
 560 the SLS is governed by the suspension system the  
 561 SLS combinations are omitted. This model is used to

**Fig. 17** Model and loads on the global model: at the top, 3'' peak wind load  $W_{3''}$ ; at the bottom left, art installation load  $G_{2,art}$ ; at bottom right, temperature load  $Temp$

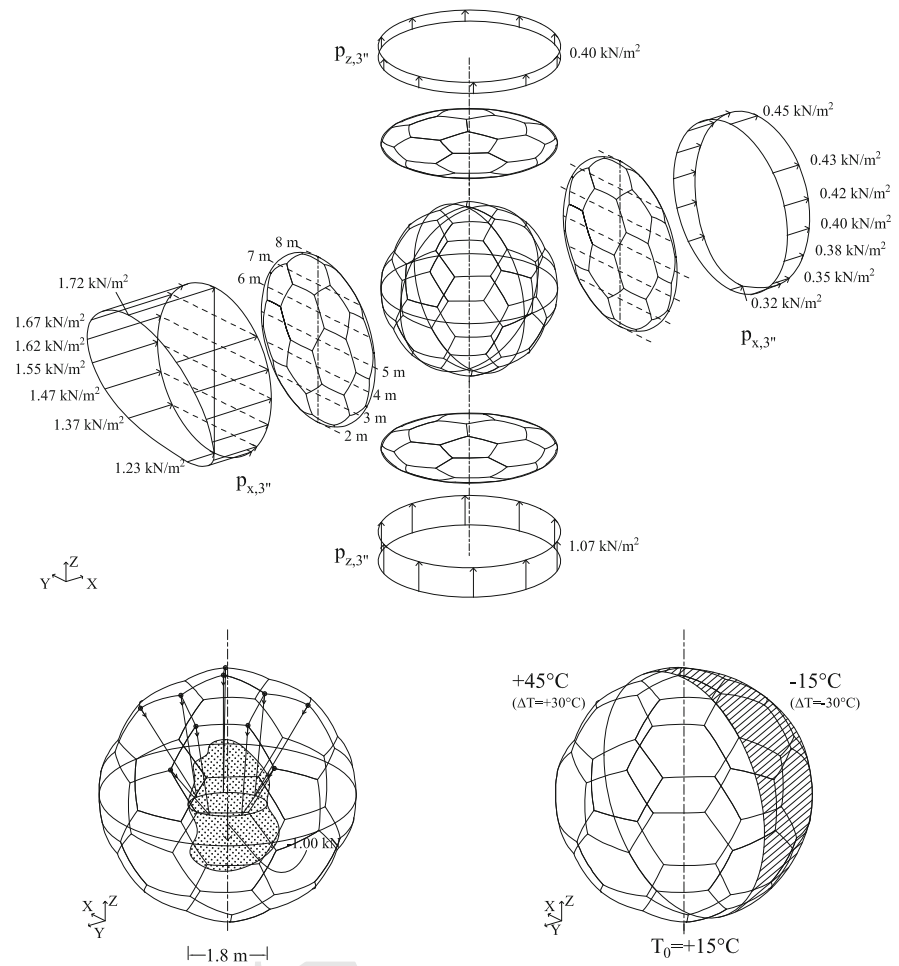


**Table 5** Coefficients for ULS load combinations employed for the structural verification of the full detailed model (ref. Sect. 5.4)

Name	$G_1$	$P$	$G_{2,art}$	$Q_{snow,sym}$	$Q_{snow,asym}$	$W_{x,10'}$	$W_{z,10'}$	$W_{x,3''}$	$W_{z,3''}$	$Q_{k,H}$	$Temp$
ULS1	1.3	1.0	1.5	1.5	0	0.9	0	0	0	0	0.9
ULS2	1.3	1.0	1.5	0	1.5	0.9	0	0	0	0	0.9
ULS3	1.3	1.0	1.5	0	1.5	0	0.9	0	0	0	0.9
ULS4	1.3	1.0	1.5	0.75	0	1.5	0	0	0	0	0.9
ULS5	1.0	1.0	0	0	0	0	1.5	0	0	0	0.9
ULS6	1.3	1.0	1.5	0	0	0	0	1.5	0	0	0.9
ULS7	1.0	1.0	0	0	0	0	0	0	1.5	0	0.9
ULS8	1.3	1.0	1.5	0.75	0	0.9	0	0	0	0	1.5
ULS9	1.3	1.0	1.5	0.75	0	0.9	0	0	0	1.5	0.9

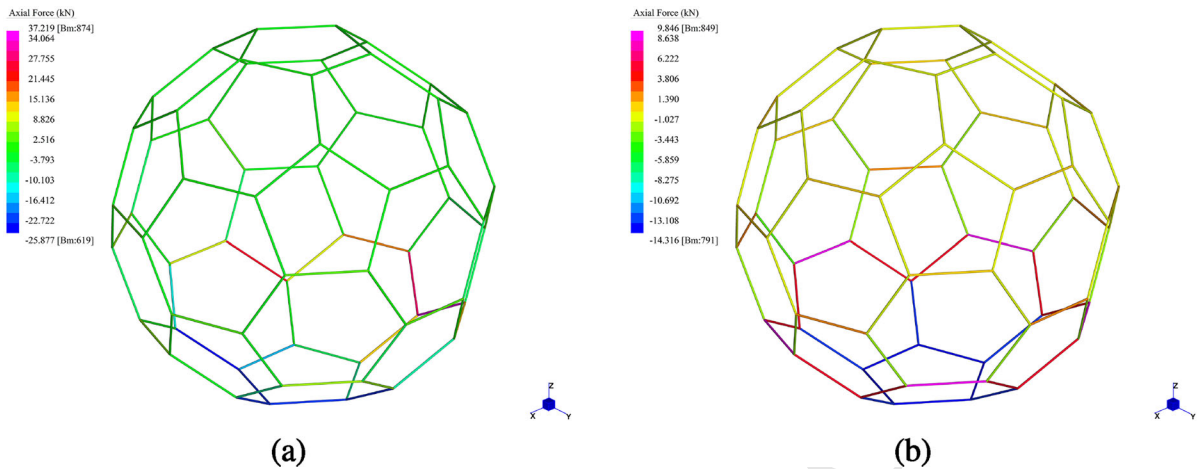


**Fig. 18** Axial forces on the rods at the ULS for the model of Fig. 15a: **a** gravity loadings; **b** prevalent 3'' X wind combination (glass elements included by means of reduced models and suspension system are hidden for output display reasons)

562 make comparison with a similar state-of-the-art struc-  
 563 ture with glued butt joints.

564 5.2 Stress and displacement results

565 As demonstrated also in the previous Sect. 4, using  
 566 a target geometry of a sphere this case study has the  
 567 advantage of highlight simultaneously different local  
 568 behavior of the components. An illustrative output is  
 569 in Fig. 18, in which are shown the axial forces on the  
 570 rods. Glass panels and the suspension system are hid-  
 571 den for output reasons. It can be deduced that for grav-  
 572 ity loading (Fig. 18a) the upper cap of the sphere is  
 573 mostly compressed with small values of axial force,  
 574 showing that glass is working in the best condition and  
 575 carries most of the shell action. On the lower side, the  
 576 panel is in convex position and its stiffness is lower,  
 577 and as demonstrated by axial forces the steel becomes  
 578 the stiffer component.

579 Same discussion can be made for the wind load com-  
 580 bination shown in Fig. 18b: rods in the wind direction  
 581 are compressed, the upper cap is still behaving as a  
 582 shell, while on the other side maximum absolute val-  
 583 ues of axial forces occur on the rods.

584 As expected, the maximum deformation achieved  
 585 at the SLS is also a function of the deformation of the  
 586 supports. This dependency is discussed in Sect. 6, how-  
 587 ever it is possible to quantify the stiffness of the struc-  
 588 ture by comparing the displacement at the SLS in the  
 589 present model (Eq. 3a) with that of the model used in

the next paragraph to measure the redundancy subject to  
 the same SLS load (Eq. 3b). Within the framework  
 of the same geometry, support and loading conditions,  
 this can be regarded as comparison of a structural shell  
 designed in accordance with the proposed concept and  
 a grid shell. It provides a measure of the contribution  
 of glass as structural material.

$$\delta_z = 11.0 \text{ mm} \leq D/500 = 12 \text{ mm} \tag{3a}$$

$$\delta_x = 32.7 \text{ mm} \leq D/180 = 33 \text{ mm}$$

$$\delta_{z,WCS} = 33.0 \text{ mm} \tag{3b}$$

$$\delta_{x,WCS} = 66 \text{ mm}$$

5.3 Redundancy

An effective measure to quantify the redundancy is  
 derived by comparing the safety factors achieved by  
 the steel components in the two models under gravity  
 loading: full model at the ULS (Fig. 18a) and WCS  
 model (Fig. 19). Table 6 shows the safety factors of the  
 most stressed steel elements in both cases. Because the  
 SGS manifests either membrane and bending forces,  
 the rods are stressed by all forces, therefore they should  
 be consequently considered in the verification.

The safety factor *SF* in the WCS model is as  
 expected lower with respect to that in the ULS. In the  
 WCS, glass is in a fractured condition, so it provides no  
 stiffness contribution but it is still able to distribute load  
 to the rods. Therefore, the deformability of the struc-

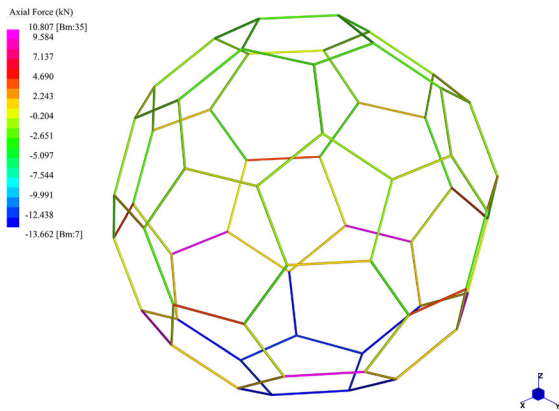


**Fig. 19** Axial forces on the WCS model at the ULS for the model of Fig. 15b (loads are applied at the nodes since the glass has no load-bearing function)

**Table 6** Safety factor  $SF$  on steel rods and redundancy  $R$  evaluation

Load case	$SF_i$	$SF_{WCS,i}$	$SF_i/SF_{WCS,i} = R$
ULS	2.94	1.02	2.88

617 ture increases with a consequent increase of bending  
 618 moments on the rods. The almost-unitary value of the  
 619  $SF_{WCS}$  reveals that the structure is still able to bear  
 620 the dead load without collapsing, and allows the oper-  
 621 ators to remove the causes of failure and to replace the  
 622 components.

623 From the ratio of the two safety factors, a redundancy  
 624 factor  $R$  of about 3 is derived, and it can be considered  
 625 a good result despite the mechanical complexity of this  
 626 case study. The value 3 bound has been assumed in  
 627 similar work (Weller et al. 2008; Laccone 2019).

628 As a matter of fact, the rods are well sized and per-  
 629 form the double function of reinforcement, as demon-  
 630 strated in asymmetric loading conditions (shown in  
 631 Fig. 18b), and of robust skeleton to avoid collapse in  
 632 extreme scenarios.

5.4 Detailed model and comparison with an all-glass structure with glued butt joints

633 The ULS performances of the SGS are quantified  
 634 through a full detailed model that includes the glass  
 635 panels as FE plate elements (Fig. 20a). The output  
 636 confirms the statics of the present structural concept:  
 637 in particular glass is mainly working as a compressed  
 638 membrane; the rods keep the joints in their position and  
 639 sustain tension load when the edge is tensioned, since  
 640 glass panels have compression-only constraints and  
 641 can escape relevant tension stress. However, maximum  
 642 principal stress occurs in the nodes' closeness but it  
 643 results within the material capacity. Although the lower  
 644 part of the sphere is less efficient because distributed  
 645 loads stress glass as a tensioned membrane, a good  
 646 safety level is maintained due to the grid of rods. In  
 647 general, these effects can be observed for all load cases.  
 648  
 649

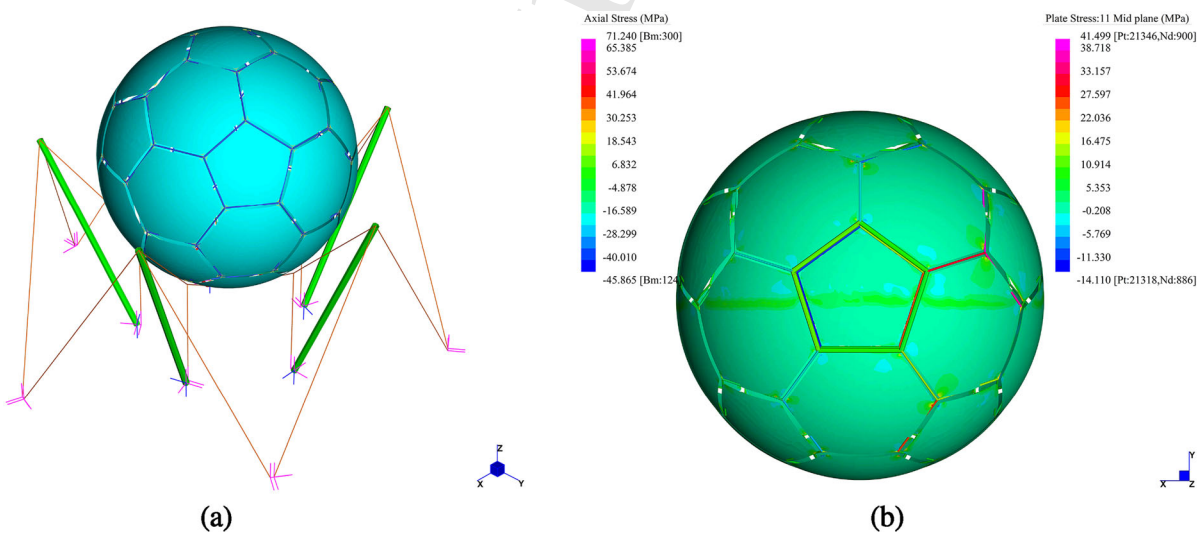


**Fig. 20** Full detailed model: **a** model; **b** ULS4 results (bottom view, the suspension system is hidden for output display reasons)



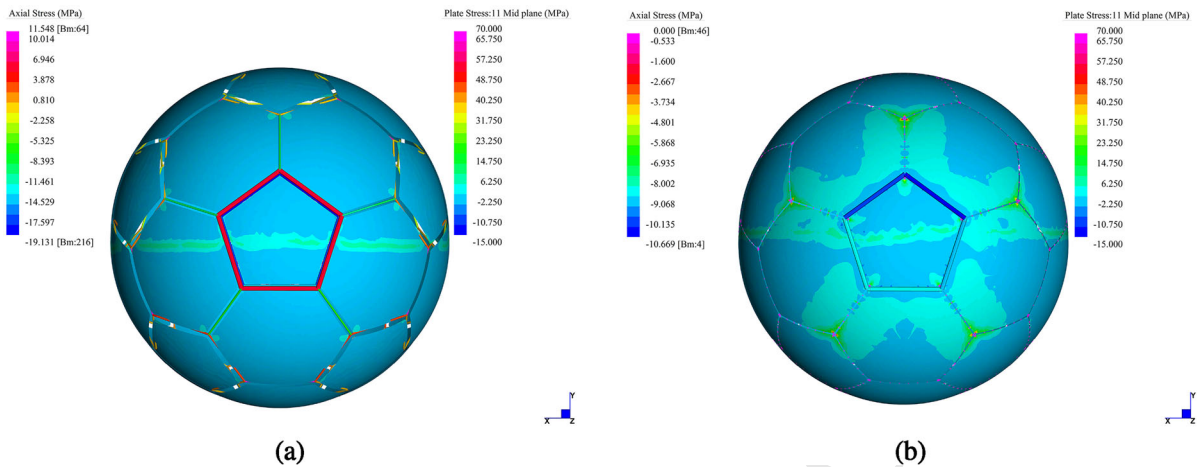


**Fig. 21** Comparison of the present concept **a** with an all-glass concept with glued butt joints **b** for the SGS geometry: results for the ULS1,  $G_{2,art}$  has not been included in the analyses (bottom view, the suspension system is hidden for output display reasons)

650 An exception is the temperature load. Since no  
 651 detailed environmental studies are used, it is supposed  
 652 to have a variation of  $\Delta T = \pm 30^\circ$  on two halves of  
 653 the surface (see as ref. Fig. 17). This loading geometry  
 654 is conventional and it is established to maximize the  
 655 stress and deformation within the loads combination.  
 656 The most remarkable effect of temperature occurs on  
 657 the ‘cold’ side of the sphere. Hence, the glass shrinkage,  
 658 which is lower than the steel, imposes a deformation on  
 659 the steel rods that force them to stretch. This effect  
 660 is mitigated by the spacers at the joints. The reverse  
 661 effect on the ‘warm’ side does not take place due to  
 662 the compression-only glass support. Lastly, the stress  
 663 induced on the panel at the transition of shadow zone  
 664 results within the material capacity.

665 The static response of this model is compared with  
 666 a similar state-of-the-art concept, which is an all-glass  
 667 shell with glued butt joints. This model adopts the same  
 668 panels’ geometry and a constant 10 mm width joint  
 669 as in Blandini’s prototype (2005) along all edges of  
 670 glass panels. The adhesive with Young’s modulus of  
 671  $E_{adh} = 1 \text{ GPa}$  is simulated with linear springs, whose  
 672 properties are deduced from the work of Bagger (2010)  
 673 (FacC\_adh1 model). There are no rods in the model,  
 674 except for the lower pentagonal ring. It constitutes the  
 675 support of the sphere and sustains tension load. To avoid  
 676 introducing punctual loads, the  $G_{2,art}$  load case is not  
 677 included. A comparison for the snow-prevailing load  
 678 combination is reported in Fig. 21. The figure reports  
 679 the elements of the bottom hemisphere and it shows that

the steel rods relieve glass from carrying tensile forces,  
 which instead using the state-of-the-art concept are sus-  
 tained more diffusely by glass. On the top hemisphere,  
 similarly in both cases, glass is mainly compressed.  
 The adoption of a steel grid has an important practical  
 outcome since it avoids the use of rigid scaffolding  
 for the panels lying, which is instead necessary for the  
 realization and curing of glued butt joints.

## 6 Influence of the suspension system

Based on the SLS results obtained from the global  
 model in Sect. 5, it appears evident that the maximum  
 horizontal and vertical displacements of the structure  
 are related to the stiffness of the suspension system.  
 Only a minimal part of the global displacement are due  
 to the deformation of the sphere. A major role is played  
 by the post-tensioning force of the cables. Figure 22  
 shows parametric plots of the maximum vertical and  
 lateral displacement of the structure with respect to the  
 applied post-tensioning force. It is evidenced that good  
 deformation parameters can be obtained by adopting a  
 value of 45 kN.

### 6.1 Modal analysis and parametric investigation on the suspended system

An additional aspect related to the suspension system  
 concerns the dependency of natural frequencies of the

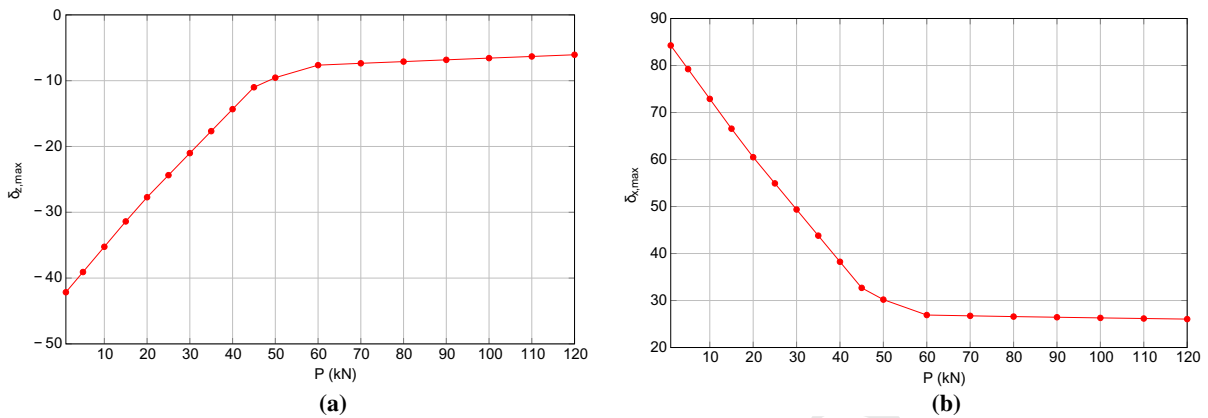


**Fig. 22** Parametric plots of the influence of the cable post-tensioning  $P$  on the maximum displacement of the SGS (a)  $\delta_{z,max}$  in the vertical and (b)  $\delta_{x,max}$  in the horizontal direction

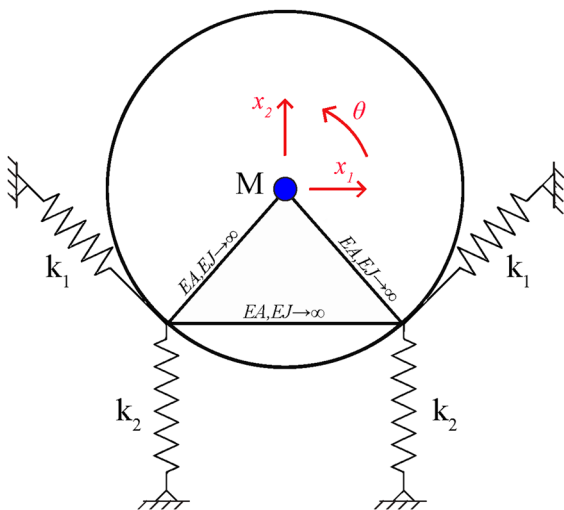


**Fig. 23** Schematic graphic representation of the 2D analytical dynamic model

The eigenvalues of the system in Eq. 5 provide the natural frequency of the non-post-tensioned system (Eq. 6).

$$\begin{cases} M\ddot{x}_1 + (k_1\sqrt{2}/2 + k_1\sqrt{2}/2)x_1 = 0 \\ M\ddot{x}_2 + (k_1\sqrt{2}/2 + k_1\sqrt{2}/2)x_2 + (k_2 + k_2)x_2 = 0 \\ \frac{1}{2}Mr^2\ddot{\theta} + (k_1r + k_1r)\theta + (k_1\frac{l}{2} + k_1\frac{l}{2})\theta = 0 \end{cases} \quad (5)$$

$$\begin{cases} f_1 = 8.35 \text{ Hz} \\ f_2 = 12.22 \text{ Hz} \\ f_3 = 16.07 \text{ Hz} \end{cases} \quad (6)$$

However this model is affected by an error of having neglected the post-tensioning induced by the weight of the structure, which will be considered in the FEM model. Building on the 2D model knowledge, a 3D model has been developed.

SGS on the post-tensioning. In order to generate these parametric plots, first a FEM 2D and then a 3D model have been created.

The 2D model exploits one of the symmetry axis and represent cumulative inertial components (mass  $M = 6600 \text{ kg}$ , rotational inertia  $I = 297 \text{ kg/m}^2$ ) and equivalent stiffness of the cables, which have been projected on the symmetry plane. The SGS is considered as a rigid body. As a 2D plane model, it has three Lagrangian parameters. To check the FEM model a simple analytical model has been developed (Fig. 23) from the dynamic equilibrium (Eq. 4).

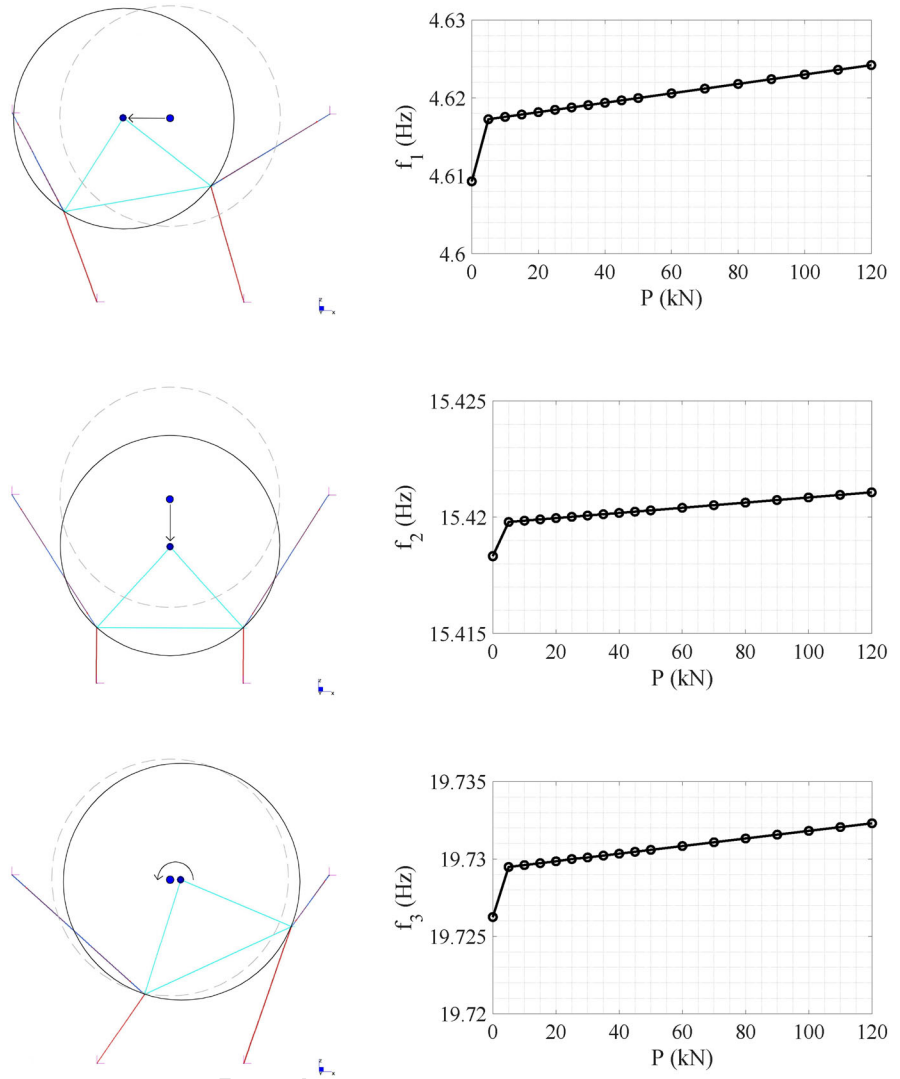
$$[M]\{\ddot{x}\} + [K]\{x\} = \{0\} \quad (4)$$

## 6.2 Results of modal analysis

The results of the parametric investigation on the natural frequencies are included in Fig. 24. It can be observed that the post-tensioning force has not a large effect on the natural frequencies. Only providing or not post-tensioning forces constitutes a remarkable modification of the system. The modal analysis on the 3D model (Fig. 25) shows results that are in line with the 2D model and are affected by the same sensitivity.

It is possible to conclude that the post-tensioning of the suspended system has to be sized in a static scenario

**Fig. 24** Parametric investigation on the effect of post-tensioning on natural frequencies using the 2D model



739 since the dynamic model is only secondary affected by  
 740 this value. In spite of this little sensitivity, a more impor-  
 741 tant outcome of the modal analysis can be traced: the  
 742 SGS considered as a rigid body has typical frequencies  
 743 of an isolated structure. Consequently, in a full dynamic  
 744 analysis of the SGS, the structural demand is supposed  
 745 to be filtered and lowered by the suspension system.  
 746 Moreover, the cables can be equipped with damping  
 747 devices to add an energy dissipation capability to the  
 748 system.

## 7 Conclusions

749  
 750 The proposed structural concept has been applied to the  
 751 case study of a 6 m-diameter suspended glass sphere  
 752 (SGS). This structure is a thin shell made of spherical  
 753 pentagonal and hexagonal panels, coupled with a grid  
 754 of straight rods. Hence, glass is used as a structural  
 755 material.

756 This case study is particularly meaningful because  
 757 it evidences the strengths of the concept. Indeed, the  
 758 geometry of the loads and the components within the  
 759 structure stresses the panels and the rods quite differ-  
 760 ently. It works best when the panels are concave and

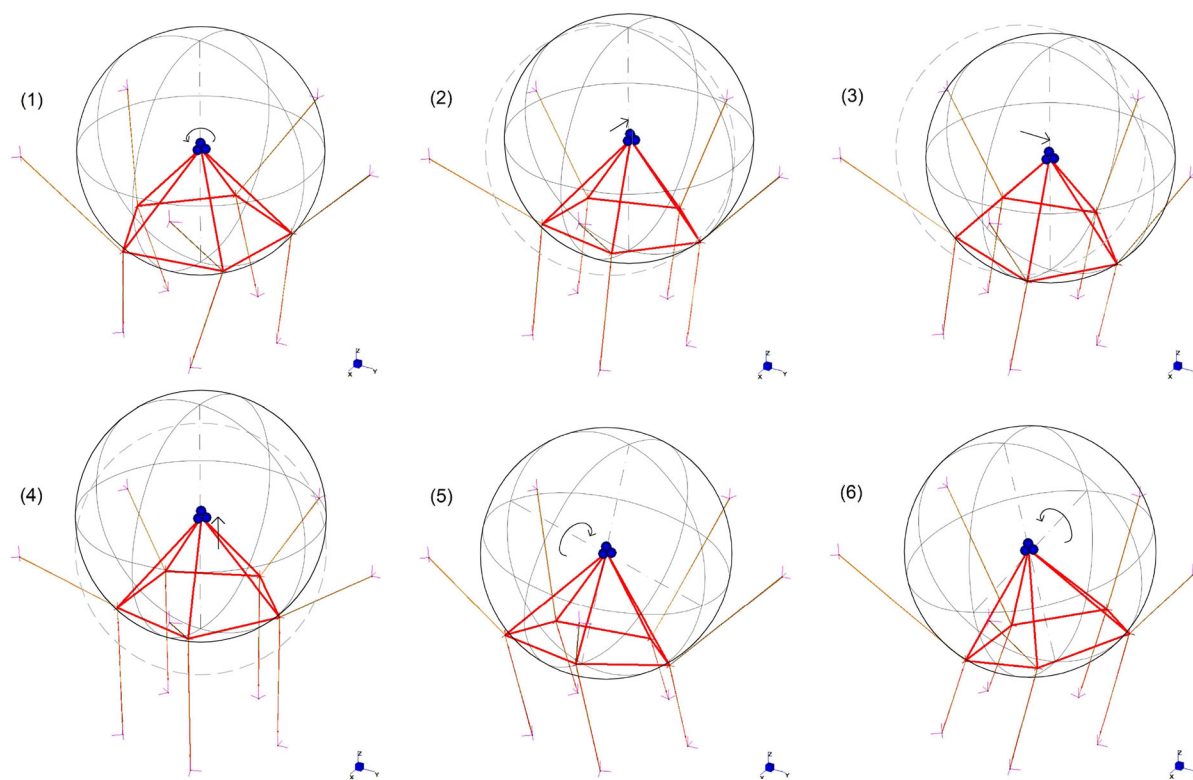


**Fig. 25** Modal analysis on the 3D model

761 well compressed, in this case the structural capacity of  
 762 glass is exploited and the rods are marginally utilized.  
 763 So, the concept appears very promising, particularly  
 764 suited for compressive structures. On the other hand,  
 765 due to the nonlinear nature of the clamping, loading  
 766 convex panels stresses more the rods. This feature is  
 767 useful also in wind suction areas or in case of asymmet-  
 768 rical loads. This makes the concept a valid alternative  
 769 with respect to the state of the art since the tensile stress  
 770 on glass lowers and accordingly the risk of cracking.

771 The redundancy concept envisages the possibility to  
 772 entrust the whole bearing capacity to the grid of rods  
 773 in an extreme scenario where the panels are simultane-  
 774 ously cracked and then able only to transfer the load  
 775 at the nodes. The validation has been performed on a  
 776 global FE model in which is observed an increase of the  
 777 bending forces on the rods that lowers the safety factor  
 778 of the grid. The ratio of the safety factors on the steel  
 779 components provides a measure of redundancy, which  
 780 reaches in this case a safe-enough level of about 3.

781 As an outcome of this holistic approach to the concep-  
 782 tual design that considers architectural and struc-

783 tural requirements, the SGS results feasible and safe.  
 784 Moreover, there are some open points that deserve fur-  
 785 ther investigation.

786 The hypothesis of a complete glass collapse is one  
 787 of the possible and more conservative scenarios, how-  
 788 ever also partial failure of panels might be considered,  
 789 and both their global and local effect. The concave  
 790 shape of the panel has an inherent robustness, and even  
 791 if cracked it may be supposed that it can develop a  
 792 membrane effect, which could still preserve the bear-  
 793 ing capacity yet with a reduced stiffness.

794 For a detailed structural design and for applications  
 795 of the concept to other shapes, considering the imper-  
 796 fection is mandatory either at global and at local level.  
 797 The node design may be updated if in this latter case  
 798 different tolerances are required. When facing detailed  
 799 design or fabrication, the control of bending geometry  
 800 will represent the major issue to deal with. It is recom-  
 801 mended to realize prototypes to be surveyed and experi-  
 802 mental validated. In general, literature on the topic of  
 803 bent glass has to be developed in order to expand its  
 804 use in architecture and as structural material. Future

805 investigation is required on several topics such as the  
806 imperfection size and shape, the buckling and the post-  
807 cracked behavior.

808 Finally, the dynamics of this structure has to be  
809 expanded on two directions: on a concept-related level  
810 to consider the dissipation capabilities of the dry-  
811 clamped glass panels, which is expected to be similar  
812 to the TVT behavior; and at the case-study system level  
813 to evaluate the isolation and dissipation capacity of the  
814 suspension system.

815 **Acknowledgements** The authors express their gratitude to  
816 Tommaso Fancelli for his collaboration to this work.

#### 817 Compliance with ethical standards

818 **Conflict of interest** The authors declare that they have no con-  
819 flict of interest.

## 820 References

- 821 Adriaenssens, S., Ney, L., Bodarwe, E., Williams, C.: Finding  
822 the form of an irregular meshed steel and glass shell based  
823 on construction constraints. *J. Archit. Eng.* **18**(3), 206–213  
824 (2012)
- 825 Bagger, A.: Plate shell structures of glass: Studies leading to  
826 guidelines for structural design. Ph.D. thesis, Technical  
827 University of Denmark (DTU) (2010)
- 828 Bedon, C., Amadio, C.: Flexural-torsional buckling: experimen-  
829 tal analysis of laminated glass elements. *Eng. Struct.* **73**,  
830 85–99 (2014)
- 831 Bedon, C., Amadio, C.: Shear glass panels with point-fixed  
832 mechanical connections: finite-element numerical investi-  
833 gation and buckling design recommendations. *Eng. Struct.*  
834 **112**, 233–244 (2016)
- 835 Bedon, C., Amadio, C.: Glass facades under seismic events  
836 and explosions: a novel distributed-tmd design concept for  
837 building protection. *Glass Struct. Eng.* **3**(2), 257–274 (2018)
- 838 Bedon, C., Belis, J., Amadio, C.: Structural assessment and  
839 lateral-torsional buckling design of glass beams restrained  
840 by continuous sealant joints. *Eng. Struct.* **102**, 214–229  
841 (2015)
- 842 Bedon, C., Louter, C.: Finite-element analysis of post-tensioned  
843 sg-laminated glass beams with mechanically anchored  
844 tendons. *Glass Struct. Eng.* **1**(1), 39–59 (2016)
- 845 Bedon, C., Zhang, X., Santos, F., Honfi, D., Kozłowski, M.,  
846 Arrighoni, M., Figuli, L., Lange, D.: Performance of struc-  
847 tural glass facades under extreme loads-design methods,  
848 existing research, current issues and trends. *Constr. Build.*  
849 *Mater.* **163**, 921–937 (2018)
- 850 Belis, J., Louter, C., Nielsen, J.H., Schneider, J.: Architectural  
851 glass. In: Musgraves, J.D., Hu, J., Calvez, L. (eds.) *Springer*  
852 *Handbook of Glass*, pp. 1781–1819. Springer, Berlin (2019)
- 853 Blandini, L.: Structural use of adhesives in glass shells. Ph.D.  
854 thesis, Institut für Leichtbau Entwerfen und Konstruieren  
855 (ILEK), Universität Stuttgart (2005)

- Blandini, L.: Prototype of a frameless structural glass shell. *Struct. Eng. Int.* **18**(3), 278–282 (2008) 856
- Bruno, L., Sassone, M., Venuti, F.: Effects of the equivalent  
857 geometric nodal imperfections on the stability of single  
858 layer grid shells. *Eng. Struct.* **112**, 184–199 (2016) 860
- Bukieda, P., Engelmann, M., Weller, B.: Testing procedure and  
861 the effect of testing machinery on four-point bending of  
862 curved glass. *ce/papers* **2**(5–6), 311–323 (2018) 863
- Bundesverband Flachglas e.V.: Guideline on thermally curved  
864 glass for building applications—BF-Bulletin 009. Tech.  
865 rep. (2011) 866
- Casagrande, L., Bonati, A., Occhiuzzi, A., Caterino, N., Auric-  
867 chio, F.: Numerical investigation on the seismic dissipation  
868 of glazed curtain wall equipped on high-rise buildings.  
869 *Eng. Struct.* **179**, 225–245 (2019) 870
- CNR: Istruzioni per la progettazione, l'esecuzione e il controllo  
871 di costruzioni con elementi strutturali di vetro. Consiglio  
872 Nazionale delle Ricerche CNR-DT 210/2012 (2012) 873
- Cupać, J., Martens, K., Nussbaumer, A., Belis, J., Louter, C.:  
874 Experimental investigation of multi-span post-tensioned  
875 glass beams. *Glass Struct. Eng.* **2**(1), 3–15 (2017) 876
- D'Ambrosio, G., Galuppi, L.: Enhanced effective thickness  
877 model for buckling of LG beams with different boundary  
878 conditions. *Glass Struct. Eng.* **5**, 205–210 (2020). <https://doi.org/10.1007/s40940-019-00116-3> 879
- Engelmann, M., Hayek, I.E., Friedreich, O., Weller, B.: Post-  
880 breakage performance of a spherical glass shell. In:  
881 *Proceedings of IASS Annual Symposia*, vol. 2017, pp. 1–6.  
882 International Association for Shell and Spatial Structures  
883 (IASS) (2017) 884
- Engelmann, M., Weller, B.: Post-tensioned glass beams for a 9 m  
885 spanning glass bridge. *Struct. Eng. Int.* **26**(2), 103–113 (2016) 886
- Feldmann, M., et al.: Guidance for European Structural Design  
887 of Glass Components. Publications Office of the European  
888 Union, Brussels (2014) 889
- Feng, Rq, Ge, Jm: Shape optimization method of free-form  
890 cable-braced grid shells based on the translational surfaces  
891 technique. *Int. J. Steel Struct.* **13**(3), 435–444 (2013) 892
- Fildhuth, T., Schieber, R., Oppe, M.: Design and construction  
893 with curved glass. *ce/papers* **2**(5–6), 369–381 (2018) 894
- Froli, M., Laccone, F.: Experimental static and dynamic tests  
895 on a large-scale free-form voronoi grid shell mock-up in  
896 comparison with finite-element method results. *Int. J. Adv.*  
897 *Struct. Eng.* **9**(3), 293–308 (2017). <https://doi.org/10.1007/s40091-017-0166-9> 898
- Froli, M., Laccone, F.: Static concept for long-span and high-rise  
899 glass structures. *J. Archit. Eng.* **24**(1), 04017030 (2018).  
900 [https://doi.org/10.1061/\(asce\)ae.1943-5568.0000285](https://doi.org/10.1061/(asce)ae.1943-5568.0000285) 901
- Froli, M., Lani, L.: Glass tensegrity trusses. *Struct. Eng. Int.*  
902 **20**(4), 436–441 (2010) 903
- Froli, M., Mamone, V.: A 12 meter long segmented post-  
904 tensioned steel-glass beam (TVT Gamma). In: Louter, C.,  
905 Bos, F., Belis, J., Lebet, J.P. (eds.) *Challenging Glass 4*  
906 & COST Action TU0905 Final Conference, pp. 243–251.  
907 CRC Press, Boca Raton (2014) 908
- Galuppi, L., Massimiani, S., Royer-Carfagni, G.: Buckling phe-  
909 nomena in double curved cold-bent glass. *Int. J. Non-Linear*  
910 *Mech.* **64**, 70–84 (2014) 911
- G+D Computing: Straus7 User's Manual (2005) 912
- G+D Computing: Using Strand7 (Straus7)—Introduction to the  
913 Strand7 Finite Element Analysis System (2010) 914

- 917 Haldimann, M., Luible, A., Overend, M.: Structural Use of  
918 Glass, vol. 10. Iabse, Zurich (2008)
- 919 Hayek, I.E., Engelmann, M., Friedreich, O., Weller, B.: Case  
920 study on a spherical glass shell. *J. Int. Assoc. Shell Spat.*  
921 *Struct.* **59**(2), 105–118 (2018)
- 922 Laccone, F.: Reinforced and post-tensioned structural glass  
923 shells: Concept, morphogenesis and analysis. Ph.D. thesis,  
924 University of Pisa (2019). [https://doi.org/10.13131/unipi/](https://doi.org/10.13131/unipi/etd/03062019-163928)  
925 [etd/03062019-163928](https://doi.org/10.13131/unipi/etd/03062019-163928)
- 926 Laccone, F., Malomo, L., Froli, M., Cignoni, P., Pietroni, N.:  
927 Automatic design of cable-tensioned glass shells. *Comput.*  
928 *Graph. Forum* **39**(1), 260–273 (2020). [https://doi.org/10.](https://doi.org/10.1111/cgf.13801)  
929 [1111/cgf.13801](https://doi.org/10.1111/cgf.13801)
- 930 Liu, Q., Huang, X., Liu, G., Zhou, Z., Li, G.: Investigation on  
931 flexural buckling of laminated glass columns under axial  
932 compression. *Eng. Struct.* **133**, 14–23 (2017)
- 933 López-Aenlle, M., Pelayo, F., Ismael, G., Prieto, M.G.,  
934 Rodríguez, A.M., Fernández-Canteli, A.: Buckling of  
935 laminated-glass beams using the effective-thickness con-  
936 cept. *Compos. Struct.* **137**, 44–55 (2016)
- 937 Louter, C., Belis, J., Veer, F., Lebet, J.P.: Structural response  
938 of SG-laminated reinforced glass beams; experimental  
939 investigations on the effects of glass type, reinforcement  
940 percentage and beam size. *Eng. Struct.* **36**, 292–301 (2012).  
941 <https://doi.org/10.1016/j.engstruct.2011.12.016>
- 942 Ludwig, J.J., Weiler, H.U.: Tragstrukturen aus Glas am Beispiel  
943 einer Ganzglastonne-Schalenkonstruktion ohne tragende  
944 Stahlunterkonstruktion am Maximilianmuseum in Augsb-  
945 urg. *Bautechnik* **77**(4), 246–249 (2000)
- 946 Luible, A., Schärer, D.: Lateral torsional buckling of glass beams  
947 with continuous lateral support. *Glass Struct. Eng.* **1**(1),  
948 153–171 (2016)
- 949 Martens, K., Caspeele, R., Belis, J.: Development of composite  
950 glass beams-a review. *Eng. Struct.* **101**, 1–15 (2015a)
- 951 Martens, K., Caspeele, R., Belis, J.: Development of reinforced  
952 and posttensioned glass beams: review of experimental  
953 research. *J. Struct. Eng.* **142**(5), 04015173 (2015b)
- 954 Martens, K., Caspeele, R., Belis, J.: Load-carrying behaviour of  
955 interrupted statically indeterminate reinforced laminated  
956 glass beams. *Glass Struct. Eng.* **1**(1), 81–94 (2016)
- Mesnil, R., Douthe, C., Baverel, O.: Non-standard patterns for  
957 gridshell structures: fabrication and structural optimization.  
958 *J. Int. Assoc. Shell Spat. Struct.* **58**(4), 277–286 (2017)
- 959 Neugebauer, J.: Applications for curved glass in buildings. *J.*  
960 *Facade Des. Eng.* **2**(1–2), 67–83 (2014)
- Pottmann, H.: *Architectural Geometry*, vol. 10. Bentley Institute  
962 Press, Crewe (2007)
- Romme, Sørvin, A., Bagger, I., Anne: Spaceplates building  
964 system. In: Cruz, P.J.D. (ed.) *Structures and Architecture:*  
965 *Concepts, Applications and Challenges*, pp. 1401–1408.  
966 CRC Press (2013)
- Santarsiero, M., Bedon, C., Moupagitsoglou, K.: Energy-based  
968 considerations for the seismic design of ductile and dissi-  
969 pative glass frames. *Soil Dyn. Earthq. Eng.* **125**, 105710  
970 (2019)
- Schlaich, J., Schober, H.: Glass-covered grid-shells. *Struct. Eng.*  
972 *Int.* **6**(2), 88–90 (1996)
- Timm, C., Chase, J.: Thermally curved glass for the building  
974 envelope. In: *Challenging Glass 4 & COST Action TU0905*  
975 *Final Conference*, p. 141. CRC Press (2014)
- Timoshenko, S.P., Gere, J.M.: *Theory of Elastic Stability*.  
977 Courier Corporation, Chelmsford (2012)
- Veer, F.A., Wurm, J., Hobbelman, G.J.: The design, construction  
979 and validation of a structural glass dome. In: *Proceedings*  
980 *of the Glass Processing Days*. Poster, 12, vol. 12 (2003)
- Villiger, J., Willareth, P., Doebbel, F., Nardini, V.: Interlocking  
982 glass spiral as building structure of the watch museum “La  
983 Maison des Fondateurs”. *Glass Struct. Eng.* **4**(1), 3–16  
984 (2019)
- Wang, X., Feng, Rq, Yan, Gr, Liu, Fc, Xu, Wj: Effect of joint  
986 stiffness on the stability of cable-braced grid shells. *Internat-*  
987 *ional Journal of Steel Structures* **16**(4), 1123–1133 (2016)
- 988 Weller, B., Reich, S., Ebert, J.: Testing on Space Grid Structures  
989 with Glass as Compression Layer. In: *Proceedings of the*  
990 *Challenging Glass Conference*, Delft, pp. 155–162 (2008)
- 991 Wurm, J.: *Glass Structures, Design and Construction of Self-*  
992 *supporting Skin*. Birkhäuser, Berlin (2007)
- 993
- Publisher’s Note** Springer Nature remains neutral with regard  
994 to jurisdictional claims in published maps and institutional affil-  
995 iations.  
996